Materials Today Communications 41 (2024) 110576

Contents lists available at ScienceDirect

Materials Today Communications

journal homepage: www.elsevier.com/locate/mtcomm

$Ti_3C_2T_x$ MXene deposition: A simple surface engineering technique for dual enhancement of biological functions for nonbearing applications

Karolina Schickle [a,*], Nima Amousa [b], Iwona Pudełko [c], Malgorzata Krok-Borkowicz [c], Elżbieta Pamuła [c], Adrian Chlanda [d], Agata Romanowska [d], Alicja Kazek-Kęsik [e,f], Kamil Drożdż [g], Jesus Gonzalez-Julian [b]

[a] Department of Restorative Dentistry and Endodontology, Justus-Liebig-University Giessen, Schlangenzahl 14, Gießen 35392, Germany
[b] Department of Ceramics, Institute of Mineral Engineering, RWTH Aachen University, Forckenbeckstraße 33, Aachen 52074, Germany
[c] Department of Biomaterials and Composites, Faculty of Materials Science and Ceramics, AGH University of Science and Technology, al. Mickiewicza 30, Kraków 30-059, Poland
[d] Łukasiewicz Research Network - Institute of Microelectronics and Photonics, Flake Graphene Research Group, Aleja Lotników 32/46, Warsaw 02-668, Poland
[e] Silesian University of Technology, Faculty of Chemistry, B. Krzywoustego Str. 6, Gliwice 44-100, Poland
[f] Silesian University of Technology, Biotechnology Centre, Krzywoustego Str. 8, Gliwice 44-100, Poland
[g] Department of Molecular Medical Microbiology, Chair of Microbiology, Faculty of Medicine, Jagiellonian University Medical College, Krakow 31-121, Poland

ARTICLE INFO

Keywords:
Biomedical implants
MXene films
Surface multifunctionalization
Cell differentiation
Bactericidal properties
Implant surface modification

ABSTRACT

Implant-associated complications, such as infection and poor osseointegration, present significant challenges in the field of biomedical implants. To address these issues, it is crucial to develop implant surfaces that possess both bacteriostatic and osteoconductive properties. In recent years, the field of surface modification for metallic substrates using two-dimensional materials has emerged as a highly promising strategy to enhance their biological properties. Among these materials, MXenes stand out as an excellent candidate for surface modifications due to their unique properties, such as biocompatibility, high specific surface area, and tunable chemical composition. In the present study, we introduce a simple deposition method of $Ti_3C_2T_x$ MXene films on SS316L substrates to improve surface-cell interactions. The differentiation study demonstrated the alkaline phosphatase (ALP) enzyme activity on $Ti_3C_2T_x$-MXene-coated samples without osteogenic medium compared to uncoated samples in both, basic and osteogenic media. Moreover, the bacteriostatic character of the deposited MXene-coatings was confirmed against Gram-positive *Staphylococcus aureus* as well as Gram-negative *Escherichia coli* bacteria. The improved stimulation of both cell osteogenic differentiation and distinctive antimicrobial features triggered by $Ti_3C_2T_x$-MXene-coatings emphasizes their great potential as implant surface modifiers to improve integration and reduce the risk of infection in various biomedical applications.

1. Introduction

Among the family of medical stainless steels, SS316L is the most commonly applied material for orthopedic and dental implant devices as well as surgical and dental instruments [1]. This is due to its biocompatibility, low allergic reactions, and non-magnetic properties to avoid interferences with sensitive devices, in combination to its excellent formability, weldability, and ductility. This enables the production of implants with complex geometries. For these reasons, SS316L finds wide applications in such medical sectors as coronary/cardiovascular stents [2,3], cranial fixation [4] orthopedic [5,6], and dental implants [7,8]. Although SS316L exhibits better corrosion resistance compared to other medical stainless steels, which can be attributed to the low carbon content (>0.03 wt%) and high chromium content (<13 wt%), the literature reports still evident degradation of this material under the harsh physiological environment, causing the release of the metallic ions and, in consequence triggering some undesired effects such as toxic reactions, thrombus formation, or cell apoptosis [9]. Thus, due to the corrosion events, the long-term biocompatibility on the interface of SS316L is strongly affected. To overcome this limitation, various methods for the deposition of protecting coatings and films on metal surfaces to improve biocompatible properties have been developed [10,

* Corresponding author.
E-mail address: Karolina.schickle@dentist.med.uni-giessen.de (K. Schickle).

https://doi.org/10.1016/j.mtcomm.2024.110576
Received 10 April 2024; Received in revised form 28 August 2024; Accepted 29 September 2024
Available online 30 September 2024

11]. Nevertheless, the need for novel, innovative, multifunctional coating materials that exhibit both, antibacterial and osseointegration properties has not yet been merged and is the focus of researchers.

In that sense, 2D materials such as graphene and its derivatives aroused interest in biocoating applications. Graphene derivatives deposited as nano-coatings on metal substrates significantly improve interfacial reactions avoiding corrosion events and enhancing interaction with the surrounding tissues [12]. Even though pristine graphene and its derivatives have become the most researched 2D-material family, their limited chemical composition and weak van der Waals bonding in multilayered systems strongly limit its possible applications. Therefore, developing the new complex 2D-structures containing more than one element, and thus offering new additional features, which can be tailored and designed in regard to the medical application field, has increasingly attracted the attention in the last years.

Among all the 2D materials, MXenes caught considerable attention due to their unique structure, flexibility in terms of chemical composition, and superior electrical, optical, magnetic and biological features [13]. The number of scientific publications in regard to these materials has been exponentially increasing since their discovering 10 years ago [14]. MXenes are commonly obtained by selective etching of the MAX phases as precursors, where "*M*" corresponds to early transition metals such as Ti, V or Cr, "*A*" is an element from the 13th or 14th element group and "*X*" represents carbon (C) or/and nitrogen (N) [13]. To obtain MXenes, the A-element of the MAX phase is selectively removed, thus the remaining general formula of MXenes is $M_{n+1}X_nT_x$, (n=1–4), where T represents the termination groups which are strongly dependent on the production process (e.g. –O, –OH, –F, –Cl). This kind of selective A-layer etching is possible owing to the weaker metallic bonds between M-A atoms, while comparing to covalently bonded M-X atoms (Fig. 1) [15].

The most common and widely literature-reported route to obtain MXenes is the chemical etching by aqueous hydrogen fluoride (HF) [16]. However, due to the aggressive character of HF, this process is not only strongly hazardous but also causes structural defects on obtained MXenes. As a result alternative mild methods based on *in-situ* HF-forming have been developed [17]. The *in-situ* HF method is one of the effective approaches to synthesizing MXenes in which the direct usage of HF can be avoided by a mixture of fluoride salts (e.g. NaF, KF, LiF) and HCl, creating an *in-situ* HF etchant. This method can produce single- or few-layer flakes with higher quality, larger lateral dimensions, fewer defects, and improved material properties in comparison with the pure HF etching method [17].

The most studied MXene, $Ti_3C_2T_X$ has already been proposed as a suitable material for tissue engineering applications due to its reactive surface and ability to further bio-modifications. It was reported, that in their free form, $Ti_3C_2T_X$-MXenes are able to enhance biological interactions with human mesenchymal stem cells [18] and human neural stem cells [19] in a manner of proliferation, differentiation, cell adhesion, and migration. Here, the applied concentration seems to be decisive, as reported by Jang and Lee [18]. Their study evidenced the cytotoxic response of human mesenchymal stem cells by higher concentrations of $Ti_3C_2T_X$ (> 50 μg/mL), while concentrations up to 20 μg/mL enhanced osteogenic differentiation. Similar concentration-dependency was observed by $Ti_3C_2T_X$ in contact with primary neural stem cells [20]. Concluding, the appropriate concentration of $Ti_3C_2T_X$–MXenes can promote differentiation processes and improve biological responses of various cells *in vitro*.

Moreover, the first evidence of $Ti_3C_2T_X$ bacteria-killing ability was reported by Rasool *et al.* [21]. Since then, extensive research has been conducted on the potential applications of MXenes as antibacterial agents in the medical field [22]. It was found that the interaction with the surrounding bacteria cells depends on the structure, size, shape, morphology, core M-X atomic constellation, and surface charge of synthesized $Ti_3C_2T_X$-MXenes. For example, the multilayered accordion-like $Ti_3C_2T_X$ structures showed lower antibacterial activity against Gram-negative *Escherichia coli* and Gram-positive *Bacillus subtilis* than the single $Ti_3C_2T_X$–nano flakes [22,23]. Shamsabadi *et al.* confirmed an antibacterial behavior of colloidal $Ti_3C_2T_x$ nanoflakes and proposed bacterial membrane damage by contact with the sharp edges of MXenes as a possible antibacterial mechanism [24]. The second most probable pathway for bacteria-killing properties is based on the surface charges of MXenes inducing the generation of the reactive oxygen species such as $O_2^{\bullet-}$, $^{\bullet}OH$, and O_2 affecting oxidative stress reactions and in consequence bacteria death [25–27].

To date, few studies have investigated how the superior biological properties of MXenes can be transferred to the surface of bulk implants. As a deposited coating, $Ti_3C_2T_x$ was applied to titanium surfaces by electrophoretic deposition [27–29]. Here, the antibacterial properties against *Staphylococcus aureus* and its methicillin-resistant *S. aureus* (MRSA) as well as the osteogenic differentiation ability of MXene-coatings were demonstrated.

In our study, we propose an efficient and simple method to deposit $Ti_3C_2T_x$ MXenes on SS316L surfaces. Merging the excellent biological properties of MXenes with the surfaces of SS316L could create a novel concept material system for a wide range of biomedical applications.

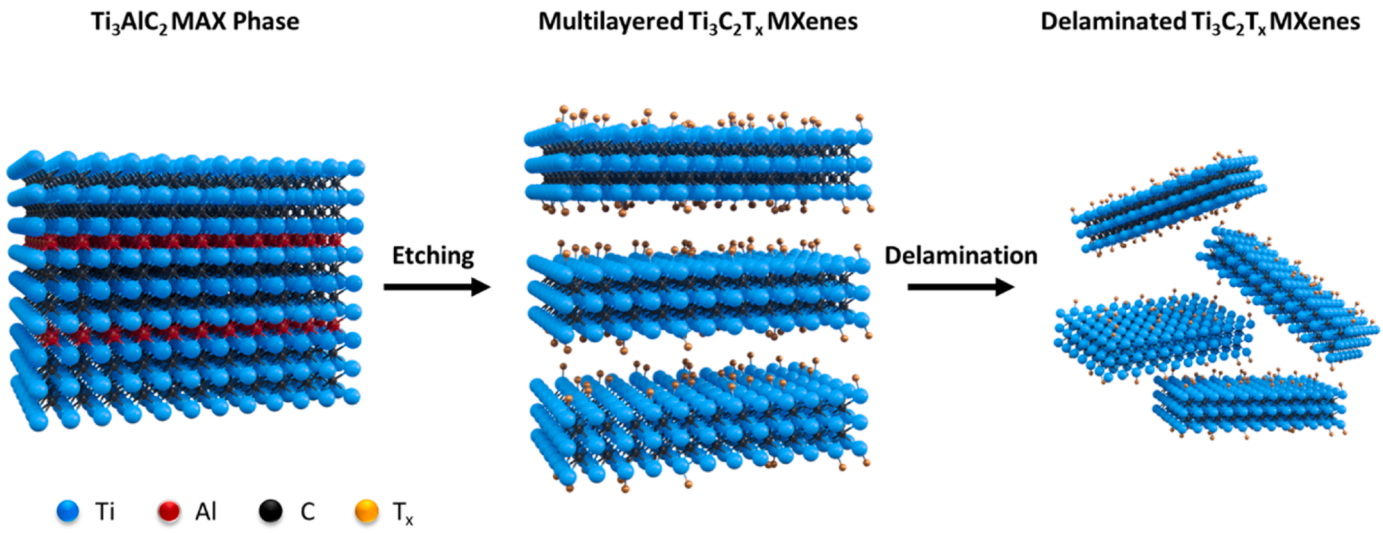

Fig. 1. Schematic illustration of MXene's synthesis from MAX phase precursor by applying selective etching method and subsequent delamination to obtain 2D nano-sheets.

Considering the flexibility provided by MXenes-composition and its tunable properties such as reactive oxygen species, surface area, surface terminations, bactericity, cytocompatibility, osseointegration, and protection against corrosion events, the processes at the interfaces of implants can be controlled and modified with respect to application requirements.

2. Material and methods

2.1. $Ti_3C_2T_x$ MXene synthesis

Ti_3AlC_2 MAX phase was used as the precursor powder for the synthesis of $Ti_3C_2T_x$ MXenes. Briefly, Ti_3AlC_2 was synthesized from its elemental constituents by solid state reaction at high temperature. Titanium (-325 mesh, 99.5 %), aluminum (-325 mesh, 99.5 %) and graphite (APS 7–11 μm, 99 %) powders (all from Alfa Aesar, Germany) were mixed in a 3:1.1:1.9 molar ratio. An extra 10 at% of aluminum was added to compensate its loss during the synthesis process at high temperature. Afterwards, the powders were heated under argon atmosphere at 5 °C/min up to 1300 °C and isothermal holding time of 3 h. The synthesized Ti_3AlC_2 pellet was ground and milled in a planetary milling for one hour in ethanol, obtaining powders with an unimodal particle size distribution and mean particle size of approx. 9 μm.

$Ti_3C_2T_x$ was prepared by selective etching of the Ti_3AlC_2 phase following the standard method [17]. The etching solution was prepared from 0.8 g of LiF (-300 mesh, Sigma Aldrich, Germany) and 10 mL of 9 M HCl (Sigma-Aldrich, 37 %). The reaction was carried out for 30 minutes at room temperature and under stirring through the aid of a magnetic bar with a rotation speed of 500 rpm. Then, 0.5 g of Ti_3AlC_2 powder was gradually dissolved into the etchant mixture at 35 °C and stirred for 24 h. Afterward, the etching product was washed several times with deionized water via centrifugation at 3500 rpm until a neutral pH was achieved. The exfoliated $Ti_3C_2T_x$ solution was then sonicated for 1 h in order to improve the delamination of $Ti_3C_2T_x$ particles. Subsequently, the solution was centrifuged at 3500 rpm for 1 h, and the supernatant containing $Ti_3C_2T_x$ flakes (~ 3 mg/mL) was collected.

2.2. MXenes immobilization on SS316L surfaces

The SS316L substrates (5 mm×5 mm x 2 mm) were first cleaned in acetone, ethanol, and double-distilled water (ddH_2O) for 15 minutes each in an ultrasonication bath (Elmasonic S 180 H, Elma, Germany). The cleaned samples were then modified by immersing them in a solution containing toluene (max 0.005 % H_2O, Merck Millipore, Germany) and 1.5 wt% 3-amino-propyl-diisopropylethoxy-silane (APDS, Abcr GmbH, Germany). The silanization process was performed in the reflux apparatus for two hours at 120 °C which is the boiling temperature of the APDS-toluene solution. The SS316L samples were then rinsed three times with toluene and ddH_2O before undergoing a one-hour post-silanization treatment at 100 °C. The MXene film was applied by dip-coating into the $Ti_3C_2T_x$ MXene solution for 1 min, rinsing with ddH_2O, and then drying overnight at 37 °C [30].

2.3. Characterization

The microstructure and elemental composition of Ti_3AlC_2 MAX phase precursor and $Ti_3C_2T_x$ MXenes were examined by scanning electron microscope (SEM, GeminiSEM 500, Zeiss, Germany) with energy dispersive X-ray (EDS) spectroscopy. The structural characteristics of the Ti_3AlC_2 phase precursor and $Ti_3C_2T_x$ MXenes were analyzed by X-ray diffraction (XRD) using an X-ray diffractometer (D8 Advance, Bruker, Germany) with Cu Kα radiation (λ = 1.54 Å). The data were collected in the 2Theta range of 3–90∘ with a 0.01° step size and 1 s/step.

Atomic force microscopy (AFM) was implemented to examine the surface of the samples. The samples were mounted directly on the microscope's working table and tested in ambient condition, in air (temp. of c.a. 21 °C and air humidity of c.a. 38 %). AFM was equipped with ACT type scanning probe with a spring constant of 37 N/m and a tip radius below 10 nm. Prior to the examination, the drive frequency of the installed scanning probe (c.a. 296 kHz) was estimated via the microscope's software. Tapping mode was used to register high-quality images of tested surfaces: five images of each sample were recorded. Acquired topographical maps were subsequently used to measure the average roughness of the surface of each type of sample. In addition, the thickness of the MXenes layer was measured by scratching the surface of coated SS316L sample with tweezers and further recording a topographical map.

Raman spectroscopy technique was used to analyze the structural properties of SS316L samples in each step during the coating process by using the Renishaw InVia spectrometer with a 532 nm laser as an excitation source. The laser power employed in the measurements was 5 %, and the spectra were collected with 5 s exposure time and 8 accumulations. The spectra for a wavenumber range of 100–800 cm-1 were averaged (5 measured spectra for coated, 5 spectra for silanized-, and 3 spectra for uncoated, using Origin software). The coated sample averaged spectrum was further analyzed in order to deconvolute constituent peaks – a sum of 11 Lorentzian peaks was fitted (curve fit function from scipy.optimize Python package).

2.4. Biological evaluation of the $Ti_3C_2T_x$ MXene film

Cytocompatibility was tested using cell culture tests with human mesenchymal stem cells from bone marrow (hMSC PromoCell, Germany). The cells were cultured on uncoated SS316L sample, coated SS316L sample with $Ti_3C_2T_x$, and on tissue culture polystyrene (TCPS) as a control in dedicated hMSC Growth Medium 2(PromoCell, Germany). The substrates were sterilized with UV light for 20 minutes and placed in 48-well plates. We seeded 10 000 cells in each well and added adequate media: basic or differentiating medium. The basic medium was prepared by mixing stem cells growth medium with the corresponding supplement (medium and supplement from PromoCell, Germany) and antibiotics (1 wt%, mixture of penicillin and streptomycin, PAN Biotech, Germany). By mixing the basic medium with ascorbic acid (1 %), β-glycerophosphate (1 %), and dexamethasone (0.02 %, all from Sigma Aldrich, Germany), we obtained differentiating medium. The same amount of wells were filled with basic and differentiating media to check the difference and the potential of materials to be used in bone tissue. Cells were cultured at 37 °C in the atmosphere of 5 % CO_2 and evaluated after 1, 3, and 7 days.

Live/dead staining was carried out to observe the morphology and viability of cultured cells. Phosphate-buffered saline (PBS) was mixed with calcein AM (0.1 %) and propidium iodide (0.1 %, all chemicals from Sigma Aldrich, Germany) and added to the wells. Plates were incubated for 20 min in darkness and after that time, we observed live and dead cells with the use of a fluorescence microscope (ZEISS Axiovert 40 CFL) with ZEISS HXP 120 C metal halide illuminator.

The viability of hMSC was checked and quantified using the AlamarBlue test. Briefly, resazurin (Sigma Aldrich, Germany) was dissolved in PBS (0.11 mg/mL) and then the solution was mixed with a medium to achieve the concentration of 10 %. The prepared solution was added to the wells and the plates were incubated for 4 h. After that time, 100 μl from each well was transferred to a black 96-well plate and the fluorescence was measured (λ_{ex}=544 nm, λ_{em}=590 nm, FluoStar OMEGA, BMG LabTech). The reduction of resazurin was calculated as follows:

$$\%resazurin\ reduction = \frac{S_x - S_{blank}}{S_{reduced} - S_{blank}} \bullet 100\%$$

S_x – fluorescence of sample

S_{blank} – fluorescence of 0 % reduced resazurin (10 % AlamarBlue reagent in medium)

$S_{reduced}$ – fluorescence of 100 % reduced resazurin (10 % AlamrBlue

reagent in medium, autoclaved)

The differentiation was investigated by measuring the quantity of alkaline phosphatase (ALP). In brief, 400 μL of the 1 % Triton X-100 solution (Sigma Aldrich, Germany) in PBS was applied to well plates and shaken for 50 minutes. Meanwhile, the working solution (WS) was prepared by dissolving 1 tablet of p-nitrophenol (Sigma Aldrich, N2765, Germany) in 20 mL of the ALP buffer. Diethanolamine (0.1 M), triton X-100 (0.1 %), and magnesium chloride hexahydrate ($MgCl_2$ 6 H_2O, 1 mM) were mixed in order to obtain ALP buffer. Later on, we transferred 25 μL of the investigated solution to a 96-well plate, added 125 μL of the WS, and left the samples to incubate for 30 min at 37C. After adding 63 μL of 1 M sodium hydroxide (NaOH) to stop the reaction, the absorbance was measured (λ = 405 nm, FluoStar Omega, BMG Labtech, Germany).

Bacterial tests. Adhesion tests of the reference bacteria *S. aureus* ATCC 25923 and *E. coli* ATCC 25922 were conducted on SS316L reference samples and SS316L coated with $Ti_3C_2T_x$ films and a control suspension of bacteria. For the experiment, a liquid medium of standard bacteria *S. aureus* ATCC 25923 was prepared at a concentration of ~ 5×10^6 CFU/mL (TSB, Biomaxima, Poland). The uncoated and MXene-coated SS316L samples were placed in a sterile culture plate and covered with 1 mL of a suspension of *S. aureus* ATCC 25923 or *E. coli* ATCC 25922 bacteria. Subsequently, the samples were incubated at 37 °C for 4 h and for 24 h for the evaluation of biofilm formation (POL-EKO, Poland). The bacterial suspension was then gently extracted and washed with sterile phosphate buffer solution (PBS, VWR, Poland). The samples were transferred to a new sterile culture plate. The next step of the study involved staining the bacteria on the samples after 4 h incubation with an aqueous solution containing SYTO9 dye (BacLight Bacterial Viability, Thermo Fisher Scientific) and observing the surface of the samples using an optical fluorescence microscope (PAULA, Leica Microsystems CMS GmbH). The area occupied by bacteria (%) was assessed using the Image J 1.54i software. The bacteria after 24 h incubation was washed with sterile phosphate buffer solution (PBS, VWR, Poland), fixed with 3 % buffered glutaraldehyde in PBS, and subsequently dehydrated by treatment with graded concentrations of ethanol solution (20, 30, 40, 50, 60, 70, 80, 90, 96, and 100 %) for 10 min each. Such prepared samples were evaluation by scanning electron microscope (SEM, GeminiSEM 500, Zeiss, Germany).

Statistical evaluation. Results of cell culture and bacterial occupied area tests are shown as average ± standard deviation (SD). OriginLab software was used to perform the statistical analysis of the data using the one-way analysis of variance (one-way ANOVA) followed by the post-hoc LSD Fisher test. For bacterial evaluation IBM SPSS Statistics 29 was applied. Statistical calculations were carried out by one-way ANOVA with post-hoc T2 Tamhane. Values of less than 0.05: $p^*<0.05$, $p^{**}<0.01$ and $p^{***}<0.001$ were considered statistically significant.

3. Results and discussion

In the present study, we introduce a simple and efficient method to deposit uniformly distributed $Ti_3C_2T_x$ films on metallic substrates. Before the characterization of the biological response, uniform and reliable $Ti_3C_2T_x$ coatings should be deposited on the metallic substrates. In our case, dip coating was selected as the processing method due to its reliability, simplicity, uniformity, reproducibility and low cost. Due to the specific biological properties of $Ti_3C_2T_x$, the proposed method allows several functions, such as cell adhesion and bactericity, that otherwise contradict each other, to be procured on one surface. First, the evidence demonstrating pure MXene synthesis without MAX phase residues was provided. Fig. 2 presents the SEM images recorded after each of the relevant steps of the synthesis process, including the Ti_3AlC_2 phase precursor (Fig. 2A), MAX phase precursor, multi-layered $Ti_3C_2T_x$, and $Ti_3C_2T_x$ nano-sheets. After the chemical etching of Al of the MAX phase precursor (Fig. 2A), a typical cluster of MXenes sheets was obtained (Fig. 2B). The MXene microstructure obtained in this study differed from the expanded accordion-like structure that typically forms due to the exothermic reaction between high concentration HF and Al between Ti-C bonds. However, the observed microstructure was resembled the structure of MXenes synthesized using low HF concentrations [17]. The compact layered structure of Ti_3AlC_2 MAX precursors was separated in multi-layered $Ti_3C_2T_x$ due to the etching process that eliminates A-atoms from the MAX phase. Such prepared multi-layered MXenes were finally delaminated to single- or few-layer $Ti_3C_2T_x$ flakes by using a simple sonication process (Fig. 2C). The significant decrease of Al after the etching process was confirmed by EDX results as the amount of aluminium in MAX powders reduced from 17.0 at. percent to less than one atomic percent in multilayered MXene powders (Table 1). As expected, due to the applied etching LiF/HCl method, F, Cl, and O elements were detected in the synthesized MXenes. These elements are typically incorporated as terminations on the nano-flakes surfaces. The obtained results are aligned with other studies that have reported the synthesis of $Ti_3C_2T_x$ MXene via selective etching of Ti_3AlC_2 MAX phase using LiF/HCl etchant [17,31]. For instance, Alhabeb *et al.* [17] reported the successful synthesis of $Ti_3C_2T_x$ MXene from Ti_3AlC_2 MAX phase using a LiF/HCl etchant. The SEM images of the $Ti_3C_2T_x$ MXene obtained in their study exhibits the opening of MXene lamellas which is

Table 1
Elemental analysis of Ti_3AlC_2 MAX precursors and $Ti_3C_2T_x$ MXene determined by EDX measurements.

Samples	Atomic %					
	Ti	C	Al	F	Cl	O
Ti_3AlC_2	51.8 ± 3.5	30.6 ± 2.7	17.1 ± 0.2	-	-	-
$Ti_3C_2T_x$	48.7 ± 2.3	20.8 ± 0.8	0.9 ± 0.2	12.8 ± 0.7	1.3 ± 0.2	15.1 ± 0.4

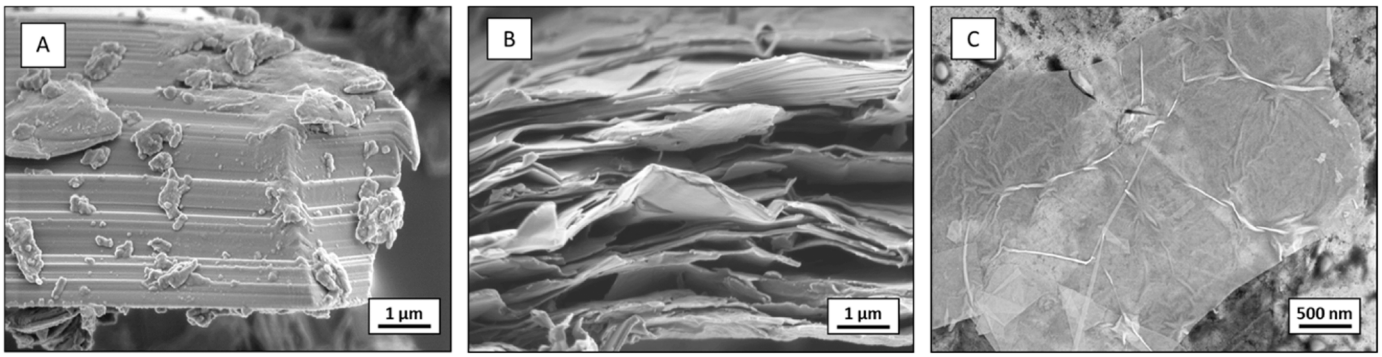

Fig. 2. SEM images of: (A) Ti_3AlC_2 MAX phase, (B) multi-layered $Ti_3C_2T_x$ MXene, and (C) delaminated $Ti_3C_2T_x$ MXene nanosheets.

comparable to what we observed in our study. Moreover, EDX analysis in both studies confirms the composition of the synthesized $Ti_3C_2T_x$ MXene.

The XRD analysis confirmed the successful synthesis of the 2D $Ti_3C_2T_x$-MXene phase after the etching procedure (Fig. 3A). The representative diffraction peak (002) of $Ti_3C_2T_x$ MXene on the XRD-spectra appears at $2\theta = 7.3°$ (shifted from $2\theta = 9.7°$ for the precursor MAX phase – Ti_3AlC_2) indicating an expansion in the interlayer spacing of $Ti_3C_2T_x$ MXene phase due to the presence of intercalant between the MXene nanosheets and introduction of functional groups [31]. Moreover, the corresponding peak of Ti_3AlC_2 at $2\theta = 39°$ was almost vanished after the etching process, indicating that the Al atomic layers were almost completely removed from the Ti_3AlC_2 MAX precursor.

Fig. 3B displays the Raman spectra of $Ti_3C_2T_x$ MXene, highlighting characteristic wave numbers indicative of its vibrational modes and surface functionalization, as reported in literature. These include in-plane and out-of-plane peaks originating from titanium and carbon atoms. The spectrum is categorized into distinct regions: the flake region, which signifies vibrations involving carbon atoms, titanium layers, and functional groups; the T_x region, which emphasizes surface functional group vibrations; and the carbon region, detailing vibrations of carbon atoms in both in-plane and out-of-plane vibrations. Following the successful synthesis of $Ti_3C_2T_x$, it was subsequently collected for coating onto SS316L after the surface modification step.

Subsequently, the MXene-coatings obtained by dip-coating were characterized. We expected to obtain homogenously distributed MXene-nano films due to the SS316L-surface activation by specific selected APDS silanization. This functionalization process was previously developed and established for graphene oxide flakes [30]. The immobilization reaction was provided by -NH_2 termination groups on SS316L substrates derived from APDS. Briefly, at one end of the molecule, the silane forms hydroxyl groups by hydrolysis, which enters into a condensation reaction with the hydroxyl groups of the SS316L substrate. When immobilized to the surface, the silanol forms a covalently bound, monomolecular layer. This silane exhibits two isopropyl groups with strong hydrophobic properties and thus ensures a protective effect for the -Si-O bonds exhibiting excellent hydrolytic stability. Moreover, these silanes do not build a network (like most silanes) on the surface but create a single bonding. The advantage is that the coating remains intact in case of single bonding failures. After substrate chemical modification by silanization, covalent immobilization of MXenes nano-flakes was performed. MXenes were covalently immobilized on the NH_2-functionalized surfaces by their –OH terminations [30].

As the first indication of surface modification, the surface morphologies of the SS316L samples were investigated by SEM as shown in Fig. 4. The polished surfaces of SS316L (Fig. 4A) could be intactly covered by homogeneously arranged MXene-films. On the SEM-image the MXene-coating, exhibiting typical wrinkle-like morphology can be observed (Fig. 4C).

Moreover, for more precise visualization of the complex topographical features of the obtained surface for biomedical applications and a better understanding of surface morphology in regard to their roughness, additionally AFM has been conducted [32,33]. The topographical images of the three samples (uncoated SS316L, silanized SS316L and coated SS316L) show subtle nanometric changes in the morphology and roughness related to subsequent stages of the conducted surface modification (Fig. 5).

Qualitative analysis of the obtained images allowed us to state that polished SS316L was characterized by a typical topography for the samples, which underwent comparable preparation protocol. The bright spots protruding from the steel surface (Fig. 5 A) should be related to post-preparation with hard particles of the implemented abrasive material. As depicted in Fig. 5B, the silanization of the steel surface resulted in alteration of the morphology of the sample, in which was also observed in the SEM evaluation (Fig. 4 B). One can notice the abundance of white particles on the surface of the modified sample. It is worth underlining that the last of the tested samples, covered with $Ti_3C_2T_x$ MXenes showed the presence of manifold flakes on its surface, visible also in SEM images (Figs. 4 and 5 C).

Taking full advantage of the capabilities offered by AFM working in tapping mode, additional data channel, the so-called phase-contrast channel, was analyzed. In general, phase-contrast can be used to distinguish surfaces differing in chemical composition and mechanical properties [34,35]. The reference sample was described by rather a uniform phase, with bright spots (different phases) recorded in the same place in the case of the topographical image. A similar observation was made for the APDS-silanized sample – the different (than the substrate) phase is exclusively related to APDS silane modification. The MXene-coated sample was characterized by a homogeneous one-phase structure, with clearly visible edges of the individual flakes immobilized to the APDS-modified stainless steel surface. Hence, it can be stated that AFM examination revealed a homogeneously distributed, intact $Ti_3C_2T_x$ MXenes layer generated on the SS316L substrate.

Roughness analysis was performed to complement the AFM measurements. SS316L exhibits the smoothest surface, with a Ra parameter of 0.69 ± 0.09 nm. After the APDS-silanization step, the average roughness increased to 2.84 ± 0.80 nm, and after the last step of the processing, the MXenes deposition, increased even further to 3.83 ± 0.39. At this point, it should be mentioned that the small standard deviation of Ra values recorded for MXene-coated suggest that a uniform and homogeneous layer of MXenes was created. In conclusion, both qualitative and quantitative analysis of AFM evaluation results clearly showed that the multi-step modification protocol described in this study guaranteed an efficient way of steel surface modification.

The last step of the AFM examination was the assessment of the thickness of the obtained MXenes layer on the scratched coatings. Based on the recorded images, the thickness of the $Ti_3C_2T_x$ flakes-based layer deposited on SS316L was approx. 450 nm (data not shown).

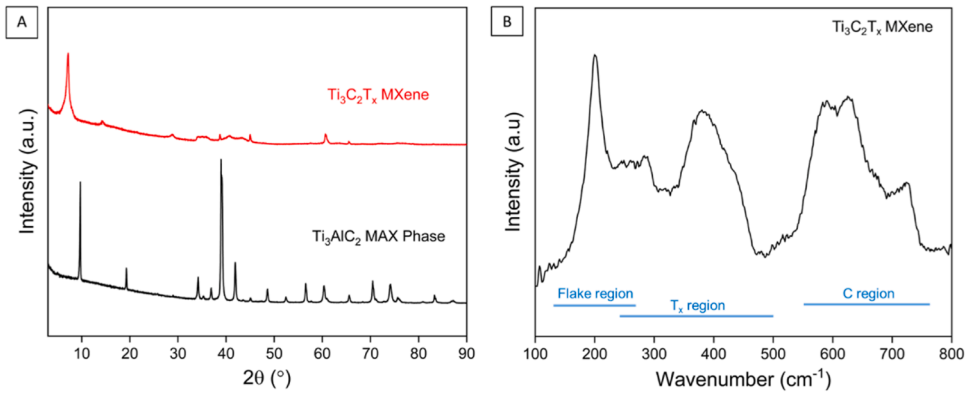

Fig. 3. (A) XRD patterns of the Ti_3AlC_2 MAX precursor and the synthesized $Ti_3C_2T_x$ MXene, and (B) Raman spectra of $Ti_3C_2T_x$ MXene.

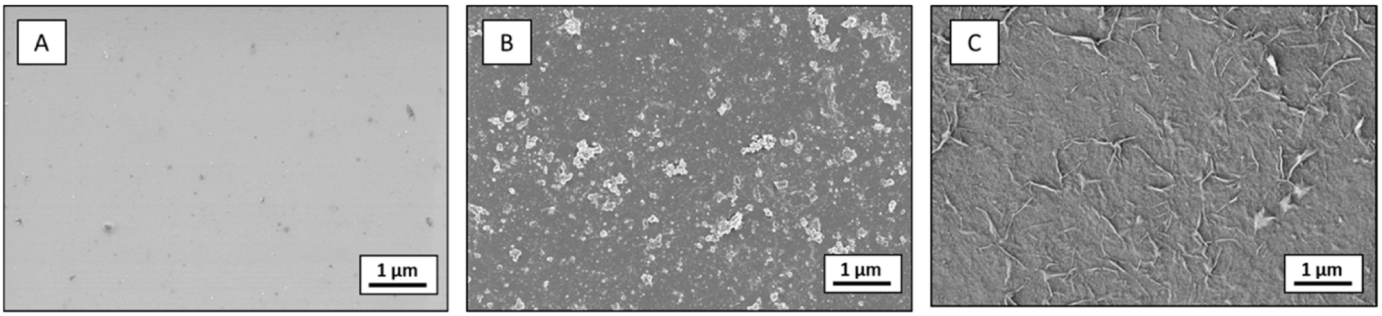

Fig. 4. SEM images of: (A) SS316L, (B) silanized SS316L, and (C) MXene-coated SS316L.

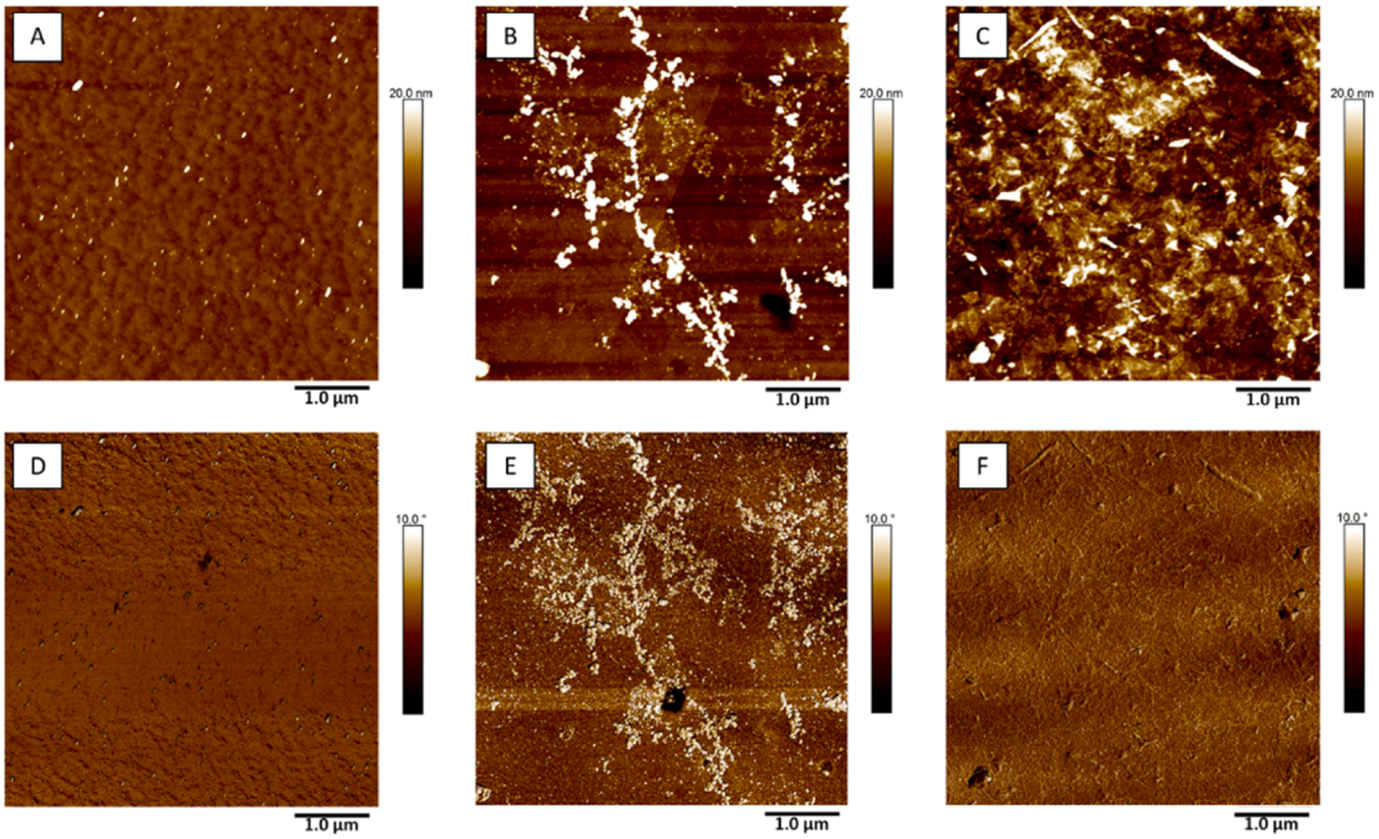

Fig. 5. AFM topographical images of the surface: (A) SS316L as a reference sample, (B) silanized SS316L, and (C) MXene-coated SS316L and AFM phase-contrast images of: (D) SS316L, (E) silanized SS316L, (F) MXene-coated SS316L.

The further evaluation of obtained modified surfaces was carried out by the Raman spectroscopy method, allows to study surface chemistry, stacking, and quality of obtained $Ti_3C_2T_x$ films. In Fig. 6, the respective Raman spectra of uncoated SS316L, silanized SS316L and MXene-coated SS316L are compared. No significant bands were observed for both uncoated SS316L and silanized SS316L samples. On the other hand in the MXene-coated sample, three main regions can be easily observed, consistently with the MXene spectrum shown in the Fig. 3B and literature data reported by A. Sarycheva and Y. Gogotsi [36]. First one, within ca. 150–250 cm^{-1} wavenumber range, refers to the flake region [35]. Second ranges between 200 and 500 cm^{-1} that can be related to the in-plane vibrations of surface groups, while the third region, between 500 and 730 cm^{-1} is linked to the carbon atoms vibrations [36]. As shown in Fig. 6 A as well as summarized in Table 2, fitted peaks were assigned. Two peaks (centered at 145 and 241 cm^{-1}) may indicate the presence of TiO_2, whereas other refer to O_2-, F_2-, $(OH)_2$- and O (OH)-terminated functional groups and corresponding carbon atoms [36–38]. The results are in accordance with the Raman spectra by applying 513 nm laser for $Ti_3C_2T_x$ MXene [36].

To verify the successful deposition of $Ti_3C_2T_x$ MXene on the 316 L SS substrates, XRD analysis was also performed on both uncoated and MXene-coated samples. The XRD patterns of the uncoated SS316L substrate displayed the characteristic peaks corresponding to the standard phases of stainless steel [39]. However, the XRD patterns of the $Ti_3C_2T_x$ MXene-coated substrate revealed also a prominent characteristic peak of $Ti_3C_2T_x$ at approximately 2θ of 7.6 degrees. This distinct peak shows the presence of the $Ti_3C_2T_x$ MXene layer on the surface of the SS316L substrate, which correlates with the AFM and Raman results. The XRD pattern of the uncoated SS316L and MXene-coated SS316L is shown in Fig. 6B.

In our study, we intend to merge the excellent multifunctional bioproperties of MXenes with a simple coating processing and commercially applied implant-materials such as SS316L to improve their biomedical performance. Thus, after the evaluation of the

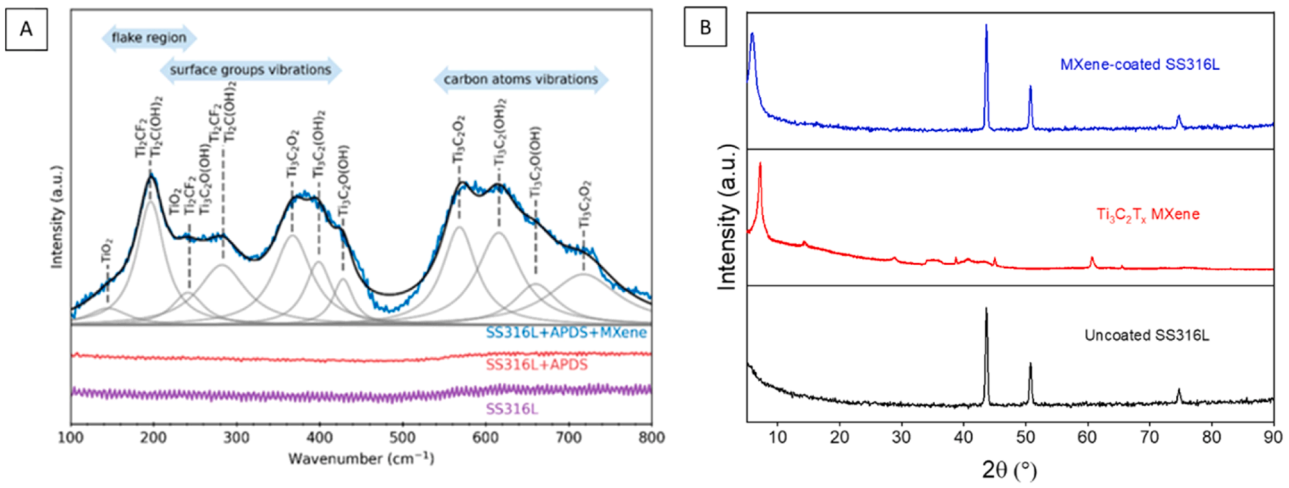

Fig. 6. (A) Raman spectra of uncoated (purple curve), silanized (red curve) and MXene-coated (blue) SS316L samples. Black line represents fitted spectrum for the coated sample and the constituent peaks are marked with grey lines. Regions consistent with Fig. 2B spectrum and literature reported data [36] can be distinguished – related to flake region, surface groups and carbon atoms vibrations, and (B) XRD pattern of the uncoated SS316L and MXene-coated SS316L.

Table 2
Peak parameters of the Raman spectra of $Ti_3C_2T_x$ films identified in accordance with literature data.

Peak position [cm^{-1}]	Identification	Source
145	TiO_2	[37]
196	Ti_2CF_2, $Ti_2C(OH)_2$,	[36,38]
241	Ti_2CF_2, TiO_2 $Ti_3C_2O(OH)$	[36,38]
282	Ti_2CF_2, $Ti_3C_2(OH)_2$	[36,38]
367	$Ti_3C_2O_2$	[36]
399	$Ti_3C_2(OH)_2$	[36]
428	$Ti_3C_2O(OH)$	[36]
568	$Ti_3C_2O_2$	[36]
616	$Ti_3C_2(OH)_2$	[36]
660	$Ti_3C_2O(OH)$	[36]
718	$Ti_3C_2O_2$	[36]

physicochemical features of the newly developed MXene-coatings on SS316L, the biological evaluation in regard to biocompatibility, differentiation potential, and further bactericidal functionalities was conducted. The preliminary cytocompatibility tests were performed by applying standard live/dead-staining according to the ISO-norm 10993–5. Here, human mesenchymal stem cells (hMSCs) viability, attachment, and growth were evaluated. Fig. 7 summarizes representative fluorescence images of hMSCs seeded on uncoated SS316L and MXene-coated SS316L surfaces after one, three, and seven days of incubation in either basic or differentiation media for cell culture. Stained cells attached to the reference sample exhibited widely spread morphologies, indicating good attachment to the substrate surfaces [40]. No significant differences were observed in the morphologies of MXene-coated samples demonstrating overall good viability.

To further quantify the viability and proliferation kinetic, AlamarBlue assays have been conducted (Fig. 8). The significantly higher amount of adhered cells were detected on the MXene-coated surfaces in both evaluated cell culture media, indicating enhanced cell-recruitment on the MXene-modified surfaces. In the basic cell culture media (Fig. 8

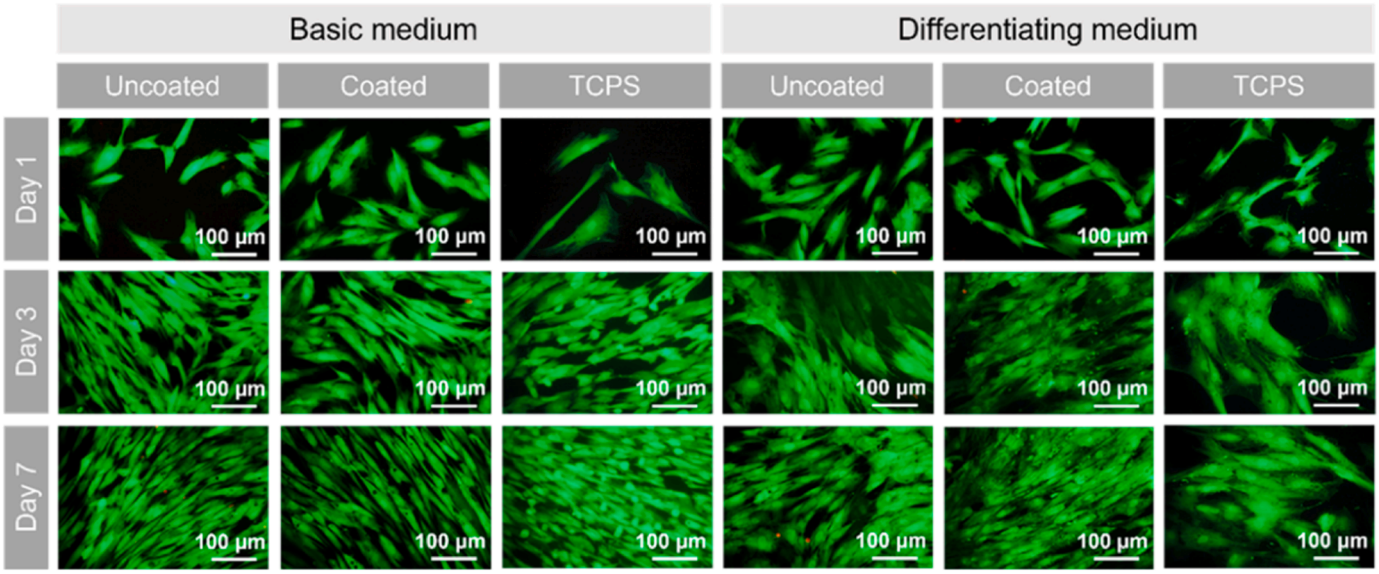

Fig. 7. Live/dead staining of human mesenchymal stem cells to assess the cytotoxicity of the SS316L uncoated samples and MXene-coated samples. Cells were incubated for 1, 3, and 7 days and then stained with calcein and PI to visualize green fluorescent viable cells and red fluorescent dead cells.

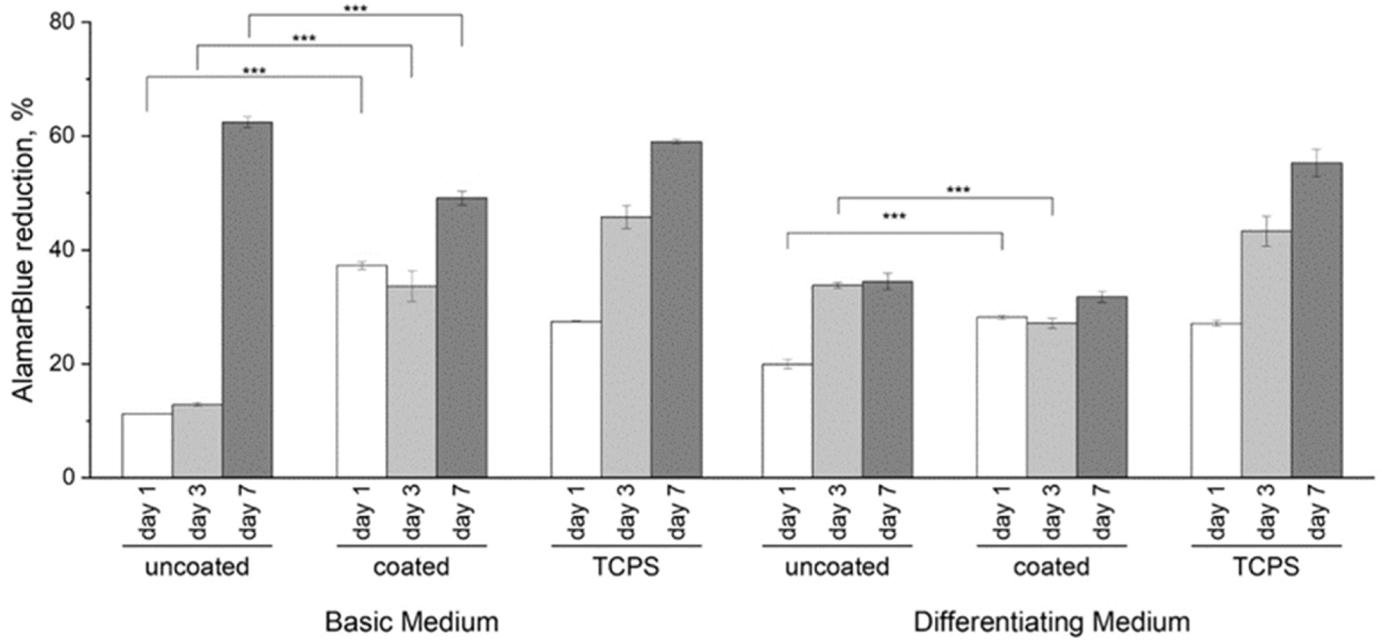

Fig. 8. hMSC cell proliferation tested by AlamarBlue. Results presented as average ± standard deviation (n = 3), statistical significance: one-way-ANOVA with Fisher LSD post hoc test, p**<0.01, p***<0.001 (in order to not clutter the figure, only significance between sample groups with and without coating was provided).

left) rather low proliferation was detected on the MXene-coated samples compared to the uncoated SS316L substrates. As expected, due to the differentiation medium, which supports differentiation but in parallel inhibits proliferation signals, low proliferation rates were measured on both, SS316L and MXene-coated substrates in the differentiation medium (Fig. 8 right).

The results of proliferation are in great accordance with the preliminary differentiation evaluation. (Fig. 9). In the basic medium, the cell mineralization was more pronounced on the MXene-coated substrates in comparison to uncoated SS316L, designating a significantly higher osteogenic differentiation potential on MXene-films. Also, in the differentiation medium, the stem cells exhibited improved osteogenic differentiation, compared to the basic medium. Moreover, here the significantly higher cell mineralization was detected again on MXene-coated substrates, showing the clear tendency of osteogenic differentiation potential of newly developed coatings. Remarkably, a significantly higher ALP signal was measured on MXene films in the basic medium than on SS316L even in the differentiation medium, demonstrating a osteogenic differentiation ability and a major influence on the hMSC-MXene interfacial interactions. The findings point to important characteristics of the MXene coating when it comes into touch with hMSC. Even though, the ALP evaluation is the first indication of possible osteogenic differentiation and the further research is required, the outcomes are highly promising.

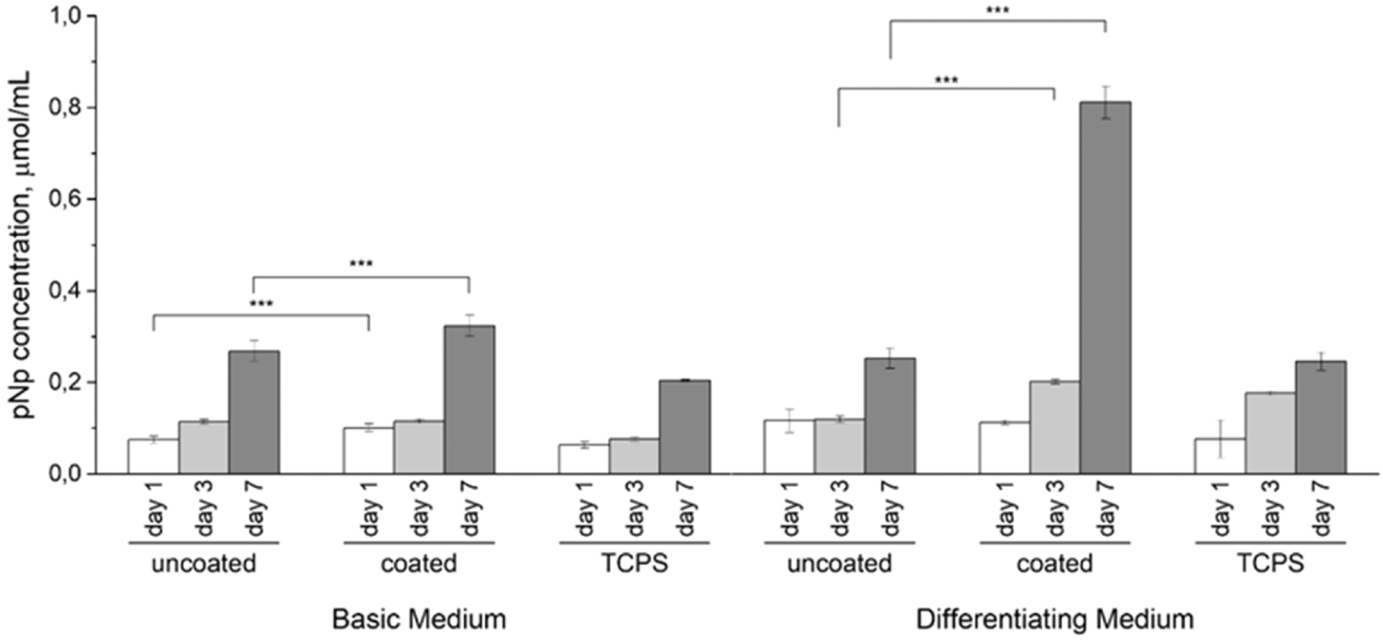

Fig. 9. Cell mineralization determined by ALP assay. Results presented as average ± standard deviation (n = 3), statistical significance: one-way-ANOVA with Fisher LSD post hoc test, p**<0.01, p***<0.001 (in order to not clutter the figure, only significance between sample groups with and without coating was provided).

The cellular responses and interactions with the surfaces are strongly influenced and controlled by the chemical composition, surface morphology, surface potential, and hydrophobicity [41]. As can be seen in Table 1, the $Ti_3C_2T_x$ flakes contain functional groups like –F, –OH, and –O, which are highly electronegative. These functional groups on the MXene-coated substrates can create a negatively charged microenvironment that can be beneficial in promoting the healing of bone defects shown in previous studies [42]. Furthermore, the negatively charged hydroxyl groups on $Ti_3C_2T_x$ may interact with proteins and create hydrogen bonds, which can further impact cell differentiation [43]. As explained in the previous parts, the typical wrinkle-like morphology was seen on the MXene-coated substrates, and the roughness of the coated samples increased in comparison to the uncoated samples. It was suggested that the wrinkled nanotopography can enhance cell-substrate interactions by providing additional attachment sites for cellular adhesion [44]. Zhang *et al.* evaluated the osteogenic activity of $Ti_3C_2T_x$ MXene films by culturing the MC3T3E1 cells on both $Ti_3C_2T_x$ MXenes films and glass as a control [45]. It was shown that the ALP activity of cells cultured on $Ti_3C_2T_x$ MXene films was considerably higher when compared to cells grown on glass, regardless of whether they were cultured in osteogenic medium or basic medium. Also, $Ti_3C_2T_x$ as nanoparticles or membranes have been already proposed as suitable materials for promoting the osteogenic differentiation of hMSC cells [46]. Jang *et al.* suggested electrophoretic deposition of $Ti_3C_2T_x$ on titanium surfaces and proved the osteogenic differentiation potential of the MXene-coatings. The results are in accordance with our findings, confirming the possible application sector for these materials.

Besides improved interaction with hMSC, an antibacterial behavior of MXene-coating has been proved. Our results confirmed antibacterial features of $Ti_3C_2T_x$ coatings against both Gram-positive *S. aureus* as well as Gram-negative *E. coli* bacteria, as presented in Fig. 10. A significant lower number of bacteria was adhered on the coated SS316L surface, especially in the case of Gram-positive bacteria. After 4 h of sample incubation with bacteria, only single *S. aureus* bacteria were adhered. Similar observation in regard to free MXene flakes was reported elsewhere [21]. This characteristic, combined with the MXene coatings' ability to enhance osteogenic differentiation of hMSCs, may contribute to reducing the risk of infection and promoting better integration of implants. The fluorescence images further support the potential of MXene-coated surfaces to inhibit bacterial growth compared to control materials—TCPS and SS316L.

A significant lower number of bacteria was adhered on the coated SS316L surface, especially in the case of Gram-positive bacteria. After 4 h of sample incubation with bacteria, only single *S. aureus* bacteria were adhered. Similar observation in regard to free MXene flakes was reported elsewhere [21]. Clinical studies suggest that *S. aureus* is the primary pathogen responsible for initiating peri-implantitis. Moreover, Li *et al.* reported results very similar to our findings, indicating that thin nanofilms generated from nanomaterials such as graphene oxide modified by lysozymes can provide both superior antibacterial activity and enhanced osteogenic differentiation [47]. This characteristic, coupled with its capacity to enhance osteogenic differentiation in human mesenchymal stem cells (hMSCs), may help inhibit the inflammatory response triggered by bacterial biofilms and, simultaneously, prevent the destruction of bone supporting the implant. The fluorescence images prove an inhibiting bacteria growth potential of MXene-coated surfaces, comparing to the control materials - TCPS and SS316L. The area occupied by bacteria was calculated based on fluorescence microscopy images (Fig. 9A). In the plots presented in Fig. 9B and C, the total area occupied by bacteria differs for *S. aureus* and *E. coli.* For the Gram-positive *S. aureus*, the total area occupied by bacteria after 4 h of incubation is the largest for the control samples (6.99 %) and comparable to those for bare SS316L and SS316L + $Ti_3C_2T_x$ (0.77 % and 0.37 %, respectively). For E. coli, the number of bacteria at the surface

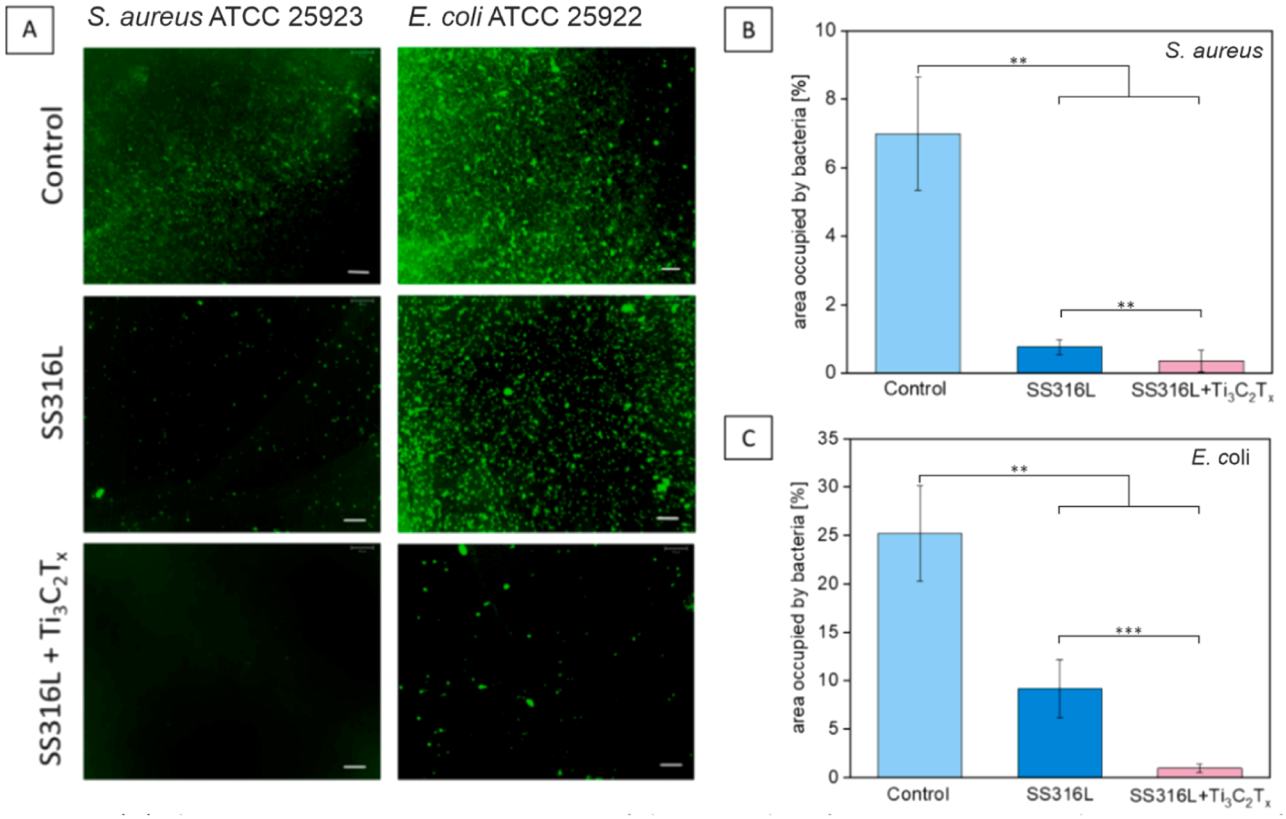

Fig. 10. (A) Fluorescence microscope images of the tested surfaces in contact with suspension of bacteria *S. aureus* ATCC 25923 or *E. coli* ATCC 25922. Scale bar corresponds to 100 μm, (B) and (C) total area occupied by *S. aureus* and *E. coli* bacteria strains after 4 h of incubation with the control, SS316L, and SS316L + $Ti_3C_2T_x$ samples. Statistical significance: one-way-ANOVA with post-hoc T2 Tamhane, p**<0.01, p***<0.001.

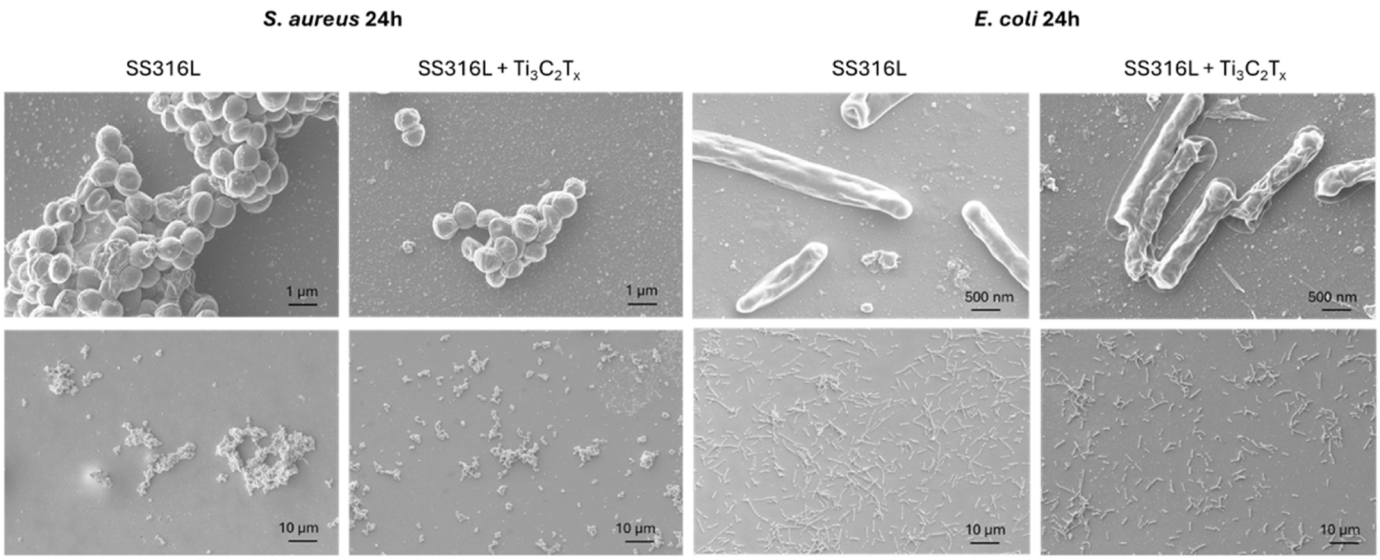

Fig. 11. Scanning electron microscope evaluation of *S. aureus* (left) and *E. coli* (right) bacteria species on SS316L and SS316L + $Ti_3C_2T_x$ samples after 24 h of incubation to evaluate biofilm formation. The morphological changes of bacteria membranes can be observed.

for the control sample (25.21 %), while for bare SS316L and SS316L + $Ti_3C_2T_x$, the total area occupied by bacteria is 9.06 % and 0.96 %, respectively. In summary, the $Ti_3C_2T_x$ MXene coating demonstrates a statistically significant strong anti-adhesion effect for both bacterial strains, with a particularly pronounced impact against Gram-negative bacteria (*E. coli*). Similar results were obtained by the research group of Shamsabadi *et al.*, who also observed reduced adhesion of bacteria on their surfaces [24]. Furthermore, SEM images after a 24-hour exposure of bacteria to the tested surfaces show alterations in bacterial morphology, particularly noticeable in Gram-negative bacteria. SEM images of bacteria post-interaction with these surfaces revealed severe membrane damage and cytoplasmic leakage, induced by the $Ti_3C_2T_x$ surfaces, emphasizing the antibacterial mechanism of these materials. Other studies have corroborated these findings, highlighting comparable changes in bacterial morphology and damage [48].

Several possible mechanisms for antibacterial events of $Ti_3C_2T_x$ MXene are proposed [21]. One of them suggests the huge specific surface area of $Ti_3C_2T_x$ with plenty of negatively charged terminations as the main triggering factor to generate a repulsive force against the negatively charged bacterial cell membrane, preventing bacteria adhesion [21]. On the other hand, the production of reactive oxygen species (ROS) by $Ti_3C_2T_x$ can also contribute to bacterial death by causing oxidative stress and, in consequence damage to the bacterial membrane [21]. Jastrzebska *et al.* indicated that the atomic structure of MXene plays an important role in determining its antibacterial activity since $Ti_3C_2T_x$ exhibited antibacterial properties in opposite to Ti_2C [48]. Nevertheless, according to the reports of antibacterial features of GO-films on conducting substrates, we suspect that due to the changes in electrical conductivity of $Ti_3C_2T_x$ MXene, the inhibited electrons transfer from bacteria membrane to the material surface is one of the most probable antibacterial mechanisms for $Ti_3C_2T_x$-SS316L junctions [49–51]. The electrical conductivity of such thin nano films is determined by their terminations and can be significantly changed due to the aging events. In the presented Raman spectra, T_x could be clearly assigned as O_2-, $(OH)_2$-, O(OH)-, and F_2- as surface terminations. Moreover, $Ti_3C_2T_x$ MXenes are susceptible to oxidation and thus, to generation of anatase TiO_2 nanocrystals integrated in amorphous C phase, as proven by Raman evaluation [52]. Formation of the new phase can negatively affect the electrical conductivity of the coating, which can be reduced from 20,000 S cm^{-1} to as low as 1 S cm^{-1} [53,54]. As a consequence, the electron transfer from bacteria membranes to the substrate may be inhibited, determining generation of the reactive oxygen species (ROS) and thus to the bacteria death. This can explain the phenomenon, that the aged $Ti_3C_2T_x$ MXenes shows improved antibacterial properties in comparison to the fresh ones [55]. However, this aspect needs to be further investigated by determining the surface potential values as a function of time/aging/oxidation state of $Ti_3C_2T_x$ MXene coatings. Although this study establishes a foundational understanding of MXene-coated SS316L surfaces as potentially antibacterial, comprehensive mechanistic studies and long-term efficacy assessments are essential for translating these findings into effective clinical solutions.

In our study, we propose a coating technique by applying MXene-nano materials. The evident stimulation of cell differentiation triggered by $Ti_3C_2T_x$-MXene coatings underlines their great potential as implant surface tuners to improve osseointegration of medical implants with reduced risk of infection development due to their unique antimicrobial properties. However, the antibacterial and osteogenic differentiation potentials at the MXene-modified interface are mutually dependent, thus a better understanding of both mechanisms, including comprehensive studies in regard to *e.g.* electron transfer, is crucial to fully control the interfacial reactions and thus to be able to translate the coatings to medical applications.

4. Conclusions

In this work, $Ti_3C_2T_x$ MXene films have been successfully immobilized on SS316L substrates using a unique and simple coating technique. The results suggest that coating SS316L with $Ti_3C_2T_x$ MXenes can be an effective approach to improving the biological properties of the surface. The samples coated with $Ti_3C_2T_x$ MXene films have shown osteogenic differentiation even without a differentiation medium, indicating its potential for enhancing bone regeneration. Furthermore, the demonstrated antibacterial activity against both Gram-positive and Gram-negative bacteria provides an additional benefit in reducing the risk of infection. Future research should further investigate the mechanisms behind these multifunctional properties and to optimize the coatings for clinical implementation.

CRediT authorship contribution statement

Kamil Drozdz: Methodology, Formal analysis, Data curation. **Jesus Gonzalez-Julian:** Writing – review & editing, Supervision, Resources, Project administration, Methodology, Funding acquisition, Formal

analysis, Conceptualization. **Iwona Pudełko-Prażuch:** Writing – review & editing, Visualization, Investigation. **Malgorzata Krok-Borkowicz:** Methodology, Investigation. **Karolina Schickle:** Writing – original draft, Supervision, Project administration, Methodology, Investigation, Funding acquisition, Conceptualization. **Nima Amousa:** Writing – review & editing, Visualization, Methodology, Investigation, Data curation, Conceptualization. **Agata Romanowska:** Visualization, Methodology, Investigation, Data curation. **Alicja Kazek-Kęsik:** Writing – review & editing, Visualization, Methodology, Investigation. **Elżbieta Pamuła:** Writing – review & editing, Supervision, Resources. **Adrian Chlanda:** Writing – review & editing, Supervision, Resources, Methodology, Investigation, Funding acquisition, Conceptualization.

Declaration of Competing Interest

The authors declare that they have no known competing financial interests or personal relationships that could have appeared to influence the work reported in this paper.

Data availability

Data will be made available on request.

Acknowledgments

This work was partially funded by the DAAD (Deutscher Akademischer Austauschdienst / German Academic Exchange Service), PPP (Programm des Projektbezogenen Personenaustauschs) 2022–2024 with Poland – project number 57602283. N.A. acknowledges the financial support for this study provided by the 'Speed Fund' program within the Profile Areas of RWTH Aachen University.

Author Agreement Statement

The authors of the publication **$Ti_3C_2T_x$ MXene deposition: A simple surface engineering technique for dual enhancement of biological functions for nonbearing applications** declare that this manuscript is original, has not been published before and is not currently being considered for publication elsewhere.

We confirm that the manuscript has been read and approved by all named authors and that there are no other persons who satisfied the criteria for authorship but are not listed. The authors further confirm that the order of authors listed in the manuscript has been approved by them.

We understand that the Corresponding Author, Dr. Karolina Schickle is the sole contact for the Editorial process. She is responsible for communicating with the other authors about progress, submissions of revisions and final approval of proofs.

References

[1] C. Morsiya, A review on parameters affecting properties of biomaterial SS 316L, Aust. J. Mech. Eng. 20 (2022) (2022) 803–813, https://doi.org/10.1080/14484846.2020.1752975.

[2] F. Airoldi, A. Colombo, D. Tavano, G. Stankovic, S. Klugmann, V. Paolillo, E. Bonizzoni, C. Briguori, M. Carlino, M. Montorfano, F. Liistro, A. Castelli, A. Ferrari, F. Sgura, C. Di Mario, Comparison of diamond-like carbon-coated stents versus uncoated stainless steel stents in coronary artery disease, Am. J. Cardiol. 93 (2004) 474–477, https://doi.org/10.1016/j.amjcard.2003.10.048.

[3] C. Bayram, A.K. Mizrak, S. Aktürk, H. Kurşaklioğlu, A. Iyisoy, A. Ifran, E. B. Denkbaş, In vitro biocompatibility of plasma-aided surface-modified 316L stainless steel for intracoronary stents, Biomed. Mater. 5 (2010) 055007, https://doi.org/10.1088/1748-6041/5/5/055007.

[4] W.C. Broaddus, K.L. Holloway, C.J. Winters, M.R. Bullock, R.S. Graham, B. E. Mathern, J.D. Ward, H.F. Young, Titanium miniplates or stainless steel wire for cranial fixation: a prospective randomized comparison, J. Neurosurg. 96 (2002) 244–247, https://doi.org/10.3171/jns.2002.96.2.0244.

[5] L. Reclaru, R. Lerf, P.Y. Eschler, J.M. Meyer, Corrosion behavior of a welded stainless-steel orthopedic implant, Biomaterials 22 (2001) 269–279, https://doi.org/10.1016/S0142-9612(00)00185-X.

[6] C.N. Kraft, B. Burian, L. Perlick, M.A. Wimmer, T. Wallny, O. Schmitt, O. Diedrich, Impact of a nickel-reduced stainless steel implant on striated muscle microcirculation: a comparative in vivo study, J. Biomed. Mater. Res 57 (2001) 404–412, https://doi.org/10.1002/1097-4636(20011205)57:3<404::aid-jbm1183>3.0.co;2-w.

[7] P. Neumann, C. Bourauel, A. Jäger, Corrosion and permanent fracture resistance of coated and conventional orthodontic wires, J. Mater. Sci.: Mater. Med. 13 (2002) 141, https://doi.org/10.1023/a:1013831011241.

[8] Y. Yonekura, K. Endo, M. Iijima, H. Ohno, I. Mizoguchi, In vitro corrosion characteristics of commercially available orthodontic wires, Dent. Mater. J. 23 (2004) 197–202, https://doi.org/10.4012/dmj.23.197.

[9] A. Rodriguez-Contreras, A. Nanci, Nanocavitation of stainless steel improves its corrosion resistance and minimizes toxic effects on MC3T3-E1 osteogenic cells, Surf. Coat. Technol.. *382* (2020) 125225, https://doi.org/10.1016/j.surfcoat.2019.125225.

[10] R. Müller, J. Abke, E. Schnell, F. Macionczyk, U. Gbureck, R. Mehrl, Z. Ruszczak, R. Kujat, C. Englert, M. Nerlich, P. Angele, Surface engineering of stainless steel materials by covalent collagen immobilization to improve implant biocompatibility, Biomaterials 26 (2005) 6962–6972, https://doi.org/10.1016/j.biomaterials.2005.05.013.

[11] A. Bandyopadhyay, I. Mitra, S.B. Goodman, M. Kumar, S. Bose, Improving Biocompatibility for Next Generation of Metallic Implants, Prog. Mater. Sci. 133 (2022) 101053, https://doi.org/10.1016/j.pmatsci.2022.101053.

[12] M.Z.I. Nizami, S. Takashiba, Y. Nishina, Graphene oxide: A new direction in dentistry, Appl. Mater. Today 19 (2020) 100576, https://doi.org/10.1016/j.apmt.2020.100576.

[13] M. Naguib, V.N. Mochalin, M.W. Barsoum, Y. Gogotsi, 25th anniversary article: MXenes: a new family of two-dimensional materials, Adv. Mater. 26 (2014) 992–1005, https://doi.org/10.1002/adma.201304138.

[14] M. Naguib, M.W. Barsoum, Y. Gogotsi, Ten years of progress in the synthesis and development of MXenes, Adv. Mater. 33 (2021) 2103393, https://doi.org/10.1002/adma.202103393.

[15] Z. Sun, D. Music, R. Ahuja, S. Li, J.M. Schneider, Bonding and classification of nanolayered ternary carbides, Phys. Rev. B. 70 (2004) m092102, https://doi.org/10.1103/PhysRevB.70.092102.

[16] O. Salim, K.A. Mahmoud, K.K. Pant, R.K. Joshi, Introduction to MXenes: synthesis and characteristics, Mater. Today Chem. 14 (2019) 100191, https://doi.org/10.1016/j.mtchem.2019.08.010.

[17] M. Alhabeb, K. Maleski, B. Anasori, P. Lelyukh, L. Clark, S. Sin, Y. Gogotsi, Guidelines for synthesis and processing of two-dimensional titanium carbide ($Ti_3C_2T_x$ MXene), Chem. Mater. 29 (2017) 7633–7644, https://doi.org/10.1021/acs.chemmater.7b02847.

[18] J.H. Jang, E.J. Lee, Influence of MXene particles with a stacked-lamellar structure on osteogenic differentiation of human mesenchymal stem cells, Mater 14 (2021) 4453, https://doi.org/10.3390/ma14164453.

[19] R. Guo, M. Xiao, W. Zhao, S. Zhou, Y. Hu, M. Liao, S. Wang, X. Yang, R. Chai, M. Tang, 2D $Ti_3C_2T_x$ MXene couples electrical stimulation to promote proliferation and neural differentiation of neural stem cells, Acta Biomater. 139 (2022) 105–117, https://doi.org/10.1016/j.actbio.2020.12.035.

[20] W. Wu, H. Ge, L. Zhang, X. Lei, Y. Yang, Y. Fu, H. Feng, Evaluating the cytotoxicity of Ti_3C_2 MXene to neural stem cells, Chem. Res. Toxicol. 33 (2020) 2953–2962, https://doi.org/10.1021/acs.chemrestox.0c00232.

[21] K. Rasool, M. Helal, A. Ali, C. Ren, Y. Gogotsi, K.A. Mahmoud, Antibacterial Activity of $Ti_3C_2T_x$ MXene, 1936-0851, ACS Nano 10 (2016), https://doi.org/10.1021/acsnano.6b00181.

[22] F. Seidi, A. Arabi Shamsabadi, M. Dadashi Firouzjaei, M. Elliott, M.R. Saeb, Y. Huang, C. Li, H. Xiao, B. Anasori, MXenes Antibacterial Properties and Applications: A Review and Perspective, Small 19 (2023) 2206716, https://doi.org/10.1002/smll.202206716.

[23] K. Rasool, K.A. Mahmoud, D.J. Johnson, M. Helal, G.R. Berdiyorov, Y. Gogotsi, Efficient antibacterial membrane based on two-dimensional $Ti_3C_2T_x$ (MXene) nanosheets, Sci. Rep. 7 (2017) 1–11, https://doi.org/10.1038/s41598-017-01714-3.

[24] A. Arabi Shamsabadi, M. Sharifian, Gh, B. Anasori, M. Soroush, Antimicrobial mode-of-action of colloidal $Ti_3C_2T_x$ MXene nanosheets, ACS Sustain. Chem. Eng. 6 (2018) 16586–16596, https://doi.org/10.1021/acssuschemeng.8b03823.

[25] Á. Serrano-Aroca, A. Cano-Vicent, i, R.S. Serra, M. El-Tanani, A. Aljabali, M. M. Tambuwala, Y.K. Mishra, Scaffolds in the microbial resistant era: Fabrication, materials, properties and tissue engineering applications, Mater. Today Bio 16 (2022) 100412.

[26] M. Rosales, A. Garcia, V.M. Fuenzalida, R. Espinoza-González, G. Song, B. Wang, J. Yu, F. Gracia, A. Rosenkranz, Unprecedented arsenic photo-oxidation behavior of few-and multi-layer $Ti_3C_2T_x$ nano-sheets, Appl. Mater. Today 20 (2020) 100769, https://doi.org/10.1016/j.apmt.2020.100769.

[27] R.P. Pandey, P.A. Rasheed, T. Gomez, K. Rasool, J. Ponraj, K. Prenger, M. Naguib, K.A. Mahmoud, Effect of sheet size and atomic structure on the antibacterial activity of Nb-MXene nanosheets, ACS Appl. Nano Mater. 3 (2020) 11372–11382, https://doi.org/10.1021/acsanm.0c02463.

[28] J.H. Jang, J.S. Oh, E.J. Lee, C.M. Han, Electophoretically deposition of Ti_3C_2 on titanium surface for hard tissue implant applications, Coat 11 (2021) 761, https://doi.org/10.3390/coatings11070761.

[29] S. Huang, Y. Fu, A. Mo, Electrophoretic-deposited MXene titanium coatings in regulating bacteria and cell response for peri-implantitis, Front. Chem. 10 (2022) 991481, https://doi.org/10.3389/fchem.2022.991481.

[30] G. Desante, N. Labude, S. Rütten, S. Römer, R. Kaufmann, R. Zybała, J. Jagiełło, L. Lipińska, A. Chlanda, R. Telle, K. Schickle, Graphene oxide nanofilm to

functionalize bioinert high strength ceramics, Appl. Surf. Sci. 566 (2021) 150670, https://doi.org/10.1016/j.apsusc.2021.150670.
[31] M. Benchakar, L. Loupias, C. Garnero, T. Bilyk, C. Morais, C. Canaff, S. Celerier. One MAX phase, different MXenes: A guideline to understand the crucial role of etching conditions on Ti3C2Tx surface chemistry. Appl. Surf. Sci. 530 (2020) 147209. https://doi.org/10.1016/j.apsusc.2020.147209 J. Halim, M.R. Lukatskaya, K.M. Cook, J. Lu, C.R. Smith, L.Å. Näslund, S.J. May, L. Hultman, Y. Gogotsi, P. Eklund, M.W. Barsoum. Transparent conductive two-dimensional titanium carbide epitaxial thin films. Chem. Mater. 26 (2014) 2374-2381. https://doi.org/10.1021/cm500641a.
[32] A. Chlanda, P. Oberbek, M. Heljak, K. Górecka, K.S. Czarnecka, M.J. Chen, Woźniak, Nanohydroxyapatite adhesion to low temperature plasma modified surface of 3D-printed bone tissue engineering scaffolds-qualitative and quantitative study, Surf. Coat. Technol. 375 (2019) 637–644, https://doi.org/10.1016/j.surfcoat.2019.07.070.
[33] M.J. Woźniak, A. Chlanda, P. Oberbek, M. Heljak, K. Czarnecka, M. Janeta, John, Binary bioactive glass composite scaffolds for bone tissue engineering—Structure and mechanical properties in micro and nano scale. A preliminary study, Micron 119 (2019) 64–71, https://doi.org/10.1016/j.micron.2018.12.006.
[34] K. Kowiorski, M. Heljak, A. Strojny-Nędza, B. Bucholc, M. Chmielewski, M. Djas, K. Kaszyca, R. Zybała, M. Małek, W. Swieszkowski, A. Chlanda, Compositing graphene oxide with carbon fibers enables improved dynamical thermomechanical behavior of papers produced at a large scale, Carbon 206 (2023) 26–36, https://doi.org/10.1016/j.carbon.2023.02.009.
[35] A. Chlanda, E. Kijeńska-Gawrońska, J. Zdunek, W. Swieszkowski, Internal nanocrystalline structure and stiffness alterations of electrospun polycaprolactone-based mats after six months of in vitro degradation. An atomic force microscopy assay, J. Mech. Behav. Biomed. Mater. 101 (2020) 103437, https://doi.org/10.1016/j.jmbbm.2019.103437.
[36] A. Sarycheva, Y. Gogotsi, Raman spectroscopy analysis of the structure and surface chemistry of $Ti_3C_2T_x$ MXene, Chem. Mater. 32 (2020) 3480–3488, https://doi.org/10.1021/acs.chemmater.0c00359.
[37] S. Zhang, M. Cai, J. Wu, Z. Wang, X. Lu, K. Li, J.M. Lee, Y. Min, Photocatalytic degradation of TiO_2 via incorporating Ti_3C_2 MXene for methylene blue removal from water, Catal. Commun. 174 (2023) 106594, https://doi.org/10.1016/j.catcom.2022.106594.
[38] T. Hu, M. Hu, Z. Li, H. Zhang, C. Zhang, J. Wang, X. Wang, Covalency-dependent vibrational dynamics in two-dimensional titanium carbides, Phys. Chem. A. 119 (2015) 12977–12984, https://doi.org/10.1021/acs.jpca.5b08626.
[39] Yukui Cai, Xichun Luo, Michelle Maclean, Yi Qin, Mark Duxbury, Fei Ding, A single-step fabrication approach for development of antimicrobial surfaces, J. Mater. Process Technol. 271 (2019) 249–260, https://doi.org/10.1016/j.jmatprotec.2019.04.012.
[40] A. Prasad, E. Alizadeh, Cell form and function: interpreting and controlling the shape of adherent cells, Trends Biotechnol. 37 (2019) 347–357, https://doi.org/10.1016/j.tibtech.2018.09.007.
[41] R.E. Baier, Surface properties influencing biological adhesion. Adhesion in Biological Systems, Acadremic Press, New York and London, 1970, pp. 15–48.
[42] X. Zhang, C. Zhang, Y. Lin, P. Hu, Y. Shen, K. Wang, S. Meng, J. Chai, X. Dai, X. Liu, X. Yun, C. Cao, S. Li, X. Deng, L. Chen, Nanocomposite membranes enhance bone regeneration through restoring physiological electric microenvironment, ACS Nano 10 (2016) 7279–7286, https://doi.org/10.1021/acsnano.6b02247.
[43] N. Ren, J. Li, J. Qiu, M. Yan, H. Liu, D. Ji, H. Liu, Growth and accelerated differentiation of mesenchymal stem cells on graphene-oxide-coated titanate with dexamethasone on surface of titanium implants, Dent. Mater. 33 (5) (2017) 525–535, https://doi.org/10.1016/j.dental.2017.03.001.
[44] K. Li, J. Yan, C. Wang, L. Bi, Q. Zhang, Y. Han, Graphene modified titanium alloy promote the adhesion, proliferation and osteogenic differentiation of bone marrow stromal cells, Biochem. Biophys. Res. Commun. 489 (2017) 187–192, https://doi.org/10.1016/j.bbrc.2017.05.124.
[45] J. Zhang, Y. Fu, A. Mo, Multilayered titanium carbide MXene film for guided bone regeneration, Int. J. Nanomed. 14 (2019) 10091–10103, https://doi.org/10.2147/IJN.S227830.
[46] J.H. Jang, E.J. Lee, Influence of MXene particles with a stacked-lamellar structure on osteogenic differentiation of human mesenchymal stem cells, Mater 14 (2021) 4453, https://doi.org/10.3390/ma14164453.
[47] M. Li, H. Li, Q. Pan, C. Gao, Y. Wang, S. Yang, S, Y. Guan, Graphene oxide and lysozyme ultrathin films with strong antibacterial and enhanced osteogenesis, Langmuir 35 (2019) 6752–6761.
[48] A.M. Jastrzębska, E. Karwowska, T. Wojciechowski, W. Ziemkowska, A. Rozmysłowska, L. Chlubny, A. Olszyna, The atomic structure of Ti_2C and Ti_3C_2 MXenes is responsible for their antibacterial activity toward E. coli bacteria, J. Mater. Eng. Perform. 28 (2019) 1272–1277, https://doi.org/10.1007/s11665-018-3223-z.
[49] K. Schickle, M. Gołda-Cępa, Z. Vuslat-Parlak, N. Grigorev, G. Desante, A. Chlanda, J. Gonzalez-Julian, Revealing bactericidal events on graphene oxide nano films deposited on metal implant surfaces, J. Mater. Chem. B 12 (2024) 2494–2504, https://doi.org/10.1039/D3TB01854G.
[50] J. Li, G. Wang, H. Zhu, M. Zhang, X. Zheng, Z. Di, X. Wang, Antibacterial activity of large-area monolayer graphene film manipulated by charge transfer, Sci. Rep. 4 (2014) 4359, https://doi.org/10.1038/srep04359.
[51] D.T. Phan, G.S. Chung, P–n junction characteristics of graphene oxide and reduced graphene oxide on n-type Si (111), Phys. Chem. Solids 74 (2013) 1509–1514, https://doi.org/10.1016/j.jpcs.2013.02.007.
[52] J. Zhu, Y. Tang, C. Yang, F. Wang, M. Cao, Composites of TiO_2 nanoparticles deposited on Ti_3C_2 MXene nanosheets with enhanced electrochemical performance, J. Electrochem. Soc. 163 (2016) A785, https://doi.org/10.1149/2.0981605jes.
[53] C. Zhang, B. Anasori, A. Seral-Ascaso, S.H. Park, N. McEvoy, A. Shmeliov, G. S. Duesberg, J.N. Coleman, Y. Gogotsi, V. Nicolosi, Transparent, flexible, and conductive 2D titanium carbide (MXene) films with high volumetric capacitance, Adv. Mater. 29 (2017) 1702678, https://doi.org/10.1002/adma.201702678.
[54] T.S. Mathis, K. Maleski, A. Goad, A. Sarycheva, M. Anayee, A.C. Foucher, K. Hantanasirisakul, C.E. Shuck, E.A. Stach, Y. Gogotsi, Modified MAX phase synthesis for environmentally stable and highly conductive Ti_3C_2 MXene, ACS Nano 15 (2021) 6420–6429, https://doi.org/10.1021/acsnano.0c08357.
[55] A. Iqbal, J. Hong, T.Y. Ko, C.M. Koo, Improving oxidation stability of 2D MXenes: synthesis, storage media, and conditions, Nano Converg. 8 (2021) 1–22, https://doi.org/10.1186/s40580-021-00259-.